



OPEN

Exploring CO₂ solubility in 1-N-butyl-3-methylimidazolium hexafluorophosphate ionic liquid using neural network models

Hadiseh Masoumi^{1✉}, Bahador Daryayehsalameh² & Ahad Ghaemi^{2✉}

In this work, [Bmim][PF₆] ionic liquid (i.e., 1-N-butyl-3-methylimidazolium hexafluorophosphate) is utilized for CO₂ capture. Since the experimental studies have their difficulty, we tried to develop multi-layer perceptron (MLP) and radial basis function (RBF) neural network models for estimating CO₂ mole fraction in [Bmim][PF₆]. The MLP with 11 hidden neurons, tangent and logarithm sigmoid activation functions in the secret and output layers, trained by the Levenberg–Marquardt algorithm, is selected as the most accurate neural network model. In the first layer, the weight matrix of temperature and pressure has been determined at 23.1182 and 2.9099, respectively. The bias vector is calculated at 15.544 in the first layer. In the second layer, the values of the weight vector and bias were determined at -1.2246 and -24.1089, respectively. It is worth noting that the MLP model provides the relative deviation of 0.0859%, 8.74%, and 30.88% for temperatures of 283.15, 298.15, and 323.15 K, respectively. The results confirmed that the MLP neural network presents higher inaccuracy for predicting CO₂ solubility at higher temperatures.

Keywords CO₂ capture, 1-N-butyl-3-methylimidazolium hexafluorophosphate, Smart modeling, MLP, RBF

Carbon dioxide (CO₂) emissions are responsible for greenhouse gases, global warming, and undesirable climate change¹. The growing human population, economic progress, industrialization, and rapid development of countries (especially India and China) make this emission dangerous. Acidic gases such as H₂S and CO₂ are produced beside light hydrocarbons in a large number of petroleum and gas production industries². Scientists warned that the greenhouse gas levels might reach such a dangerous level that they can not be reversed at all³. Therefore, reducing CO₂ emissions is one of the main concerns for continuing our life on the earth in the current century. Different solvents⁴ are applied for absorbing CO₂ gas, such as amine solutions⁵, amino acid salt⁶, eutectic solvent⁷, brine⁸, and ionic liquids⁹. However, amine solutions have drawbacks, especially high evaporation loss, accumulation of water in the gas phase, and the release of corrosive side materials. Besides the solvent type, information about the phase behavior of solvents, like solubility parameters, can help researchers to improve the absorption procedure. Ionic liquids are a new group of environmentally friendly solvents. The disadvantages of the amine solutions are not observed in the ionic liquid, especially when generating the pollutant vapors during applications. Moreover, ionic liquids have the potential to dissolve many diverse materials, such as organic, inorganic, and organometallic compounds. The research studies conducted on CO₂ capture by ionic liquids have experimental and modeling types. Researchers focused on experimental measurements of CO₂ solubility in 1-butyl-3-methylimidazolium chloride¹⁰, 1-butyl-3-methylimidazolium acetate¹¹, 1-butyl-3-methylimidazolium methyl sulfate¹¹, 1-methyl-1-propylpyrrolidinium dicyanamide¹², 1-ethyl-3-methylimidazolium acetate¹², 1-octyl-3-methylimidazolium tetrafluoroborate¹³, and 1-N-butyl-3-methylimidazolium hexafluorophosphate¹⁴. Highlighting the difficulty, economic cost, and reproducibility of an experimental study, some researchers attempted to present a network for anticipating the CO₂ mole fraction in ionic liquids. Indeed, machine learning approaches like ANN, Grey Wolf optimization, Whale optimization, and Gravity search optimization algorithms¹⁵, multivariate adaptive regression⁸, and adaptive network-based fuzzy inference systems (ANFIS)¹⁶ are appropriate tools for predicting gas solubility. ANN helps anticipate data. ANN is one of the crucial programs^{17,18} and a part of artificial intelligence that generates a trend of the human nervous system regarding the obtained values in the laboratory. Companies such as petroleum which generate

¹Department of Applied Chemistry, Faculty of Chemistry and Petroleum Sciences, Bu-Ali Sina University, Hamedan 6517838683, Iran. ²School of Chemical, Petroleum and Gas Engineering, Iran University of Science and Technology, P.O. Box: 16765-163, Tehran, Iran. ✉email: h.masoumi@basu.ac.ir; aghaemi@iust.ac.ir

huge amount of CO₂ gases can employ proficient chemical engineers in the field of ANN for predicting the CO₂ solubility in diverse temperatures, pressures, etc., with use of suggested formulations of ANN program without spending much investment in installing advanced equipment, hiring labors, purchasing materials, and consuming electricity or heat. Thus, ANN can intensely help the industries in terms of costs and economic aspects. Some conducted works in the application of ANN for the absorption of CO₂ with ionic liquids have been listed in Table 1. The objective of this work is to model the CO₂ solubility with the help of an ANN. For this purpose, two ANN models were utilized, including a multilayer perceptron (MLP) and a radial basis function (RBF). Temperature and pressure were considered as inputs of the ANN in this work. Additionally, the impacts of temperature and pressure on the CO₂ mole fraction were studied. The limitations of the previous work can be referred to in this note, that they have not studied only one type of ionic liquid ([Bmim][PF₆]) in the adsorption of CO₂ gas at different temperatures and pressures. The main purpose of this work is to use artificial intelligence for detecting the best temperature and pressure at which [Bmim][PF₆] ionic liquid performance becomes high in trapping CO₂ molecules. The other main purpose is finding the most appropriate ANN structure for predicting the solubility of CO₂ in [Bmim][PF₆] at every temperature and pressure without spending cost and time in the laboratory.

Experimental databank

ANNs are among the data-driven methodologies. This means that they obtain their understanding of the corresponding process from experimental measurements. Therefore, collecting an experimental database is necessary to develop the ANN-based paradigm for predicting CO₂ mole fraction in the [Bmim][PF₆]. For this aim, a relatively huge database having 371 datasets is gathered from thirteen different experimental studies^{30–42}. Table 2 presents the work's independent and dependent variables, their ranges, and the number of collected datasets from different references. In summary, our databank covers temperatures of 283.15 to 546.15 K, pressures of 0.092 to 196.8 bar, and CO₂ solubility of 0.001 to 0.721. To provide readers with visual observation, the histogram of temperature, pressure, and CO₂ mole fraction in the [Bmim][PF₆] is shown in Figs. 1S to 3S (supplementary section), respectively. It is essential to note that the histogram is a popular method to understand how many data points are available in any specific range of a considered domain. The x-axis divides the whole domain of a given variable into several segments, while its y-axis shows the number of available data points in each segment. Figs. 1S and 2S (supplementary section) show that significant parts of the collected experimental database were conducted at small temperatures and pressures. It is not hard to observe that more than 310 datasets cover temperatures < 350 K, and only 51 data points are available for the higher temperatures. Moreover, large numbers of our collected datasets (~220 data points) cover pressures smaller than 20 bar. On the other hand, despite the pressure and temperature data points, the collected CO₂ solubility measurements have a better distribution. They are almost uniformly distributed over the available domain.

Theory and methodology

The fundamentals of ANNs as intelligent mathematical models are tried to be explained in this section. Moreover, the structure of multi-layer perceptron (MLP) and radial basis function (RBF) neural networks is also concisely reviewed. The main differences between these two types of ANN methodology are related to their activation function and training procedure.

ANN theory

ANNs are the learnable mathematical paradigms constructed by simulating the biological neuron operation⁴³. Equations (1) and (2) explain all computational operations conducted by the neurons.

Researcher	Temperature (K)	Pressure (kPa)	No. of data	No. of ionic liquids	Output	Output range	Type of neural network	Refs.
Eslamimanesh et al	313.15–636.3	0.1–971	1128	24	CO ₂ solubility	2.02e ⁻⁶ –8.379e ⁻¹	Three-Layer Feed Forward Neural Networks (3FFNN)	19
Gholizadeh & Sabzi	298.15–348.15	0–2000	350	35	CO ₂ sorption	0.0326–115.2124	FFANN	20
Baghban et al	298.15–373.15	9.9–100.12e ³	728	14	CO ₂ solubility	0.165–0.824	multi-layer perceptron artificial neural network (MLP-ANN)- adaptive neuro-fuzzy inference system (ANFIS)	21
Venkatraman & Alsberg	271–413	0–957e ⁴	10,000	185	CO ₂ solubility	0–1.16	random forest model	22
Tatar et al	298.15–373.15	0.0097–100.12	728	14	CO ₂ solubility	0.00284–0.824	MLP & radial basis function (RBF)	23
Hamzehie et al	298–373.2	4–20,100	733	32	CO ₂ solubility	0–3	back-propagation algorithm	24
Fierro et al	273.15–449.41	10–100,120	2099	33	CO ₂ solubility	0.1–0.8456	MLP	25
Nassef	303–333	200–3000	20	1	CO ₂ solubility	0.48–0.67	ANFIS	26
Wang et al	298.15–338.15	0–8000	768	4	CO ₂ mole fraction	0–0.6	support vector machine (SVM)	27
Ali et al	243.2–453.15	0.798–49,900	10,116	124	CO ₂ solubility	0–1	Long short-term memory (LSTM)	28
Rahimi et al	298.097–343.249	9660–1,900,790	173	7	CO ₂ mole fraction	0.140–40.620	MLP-RBF	29

Table 1. The conducted investigations in the absorption of CO₂ using the ANN method.

Independent variables		Dependent variable	No. of data	References
Temperature (K)	Pressure (bar)	CO ₂ solubility (mole fraction)		
283.15–323.15	0.49–13.05	0–0.02	77	30
298.15–333.15	5.66–146.43	0.09–0.64	43	31
313.15–393.15	0.09–9.61	0.01–0.55	36	32
298.00–298.00	0.10–20	0–0.28	9	33
333.15–333.15	14.29–92.53	0.22–0.66	7	34
313.2–333.2	7.21–196.80	0.05–0.72	60	35
283.2–348.2	4.07–20.19	0.03–0.37	24	36
283.15–393	0.48–97.34	0.01–0.55	62	37
293–393	0.55–1.84	0–0.02	20	38
313.15–313.15	21.67–82.43	0.23–0.54	9	39
333–333	46.60–102.33	0.29–0.49	4	40
298–323.15	4.98–20.02	0.05–0.29	12	41
546.15–546.15	2.90–83.37	0.01–0.28	8	42

Table 2. Summary of the gathered database for CO₂ solubility in [Bmim][PF₆] ionic liquid.

$$\text{net} = \sum_{i=1}^N w_{mi} x_i + b_m \quad (1)$$

$$\text{out}_m = f(\text{net}) \quad (2)$$

These equations express that the entry signal (x_i) is multiplied by the adjustable parameters, namely, weights (w_{mi}), and then added to another tunable parameter, i.e., bias (b_m). This linear mathematical operation should pass through an activation function (f) to generate the output signal (out_m). The rationale for model selection is based on the statistical analysis, especially relative deviation and correlation coefficient values, which display the closeness of experimental data to the given model.

MLP network

MLP, which is categorized as a feed-forward neural network. It should be mentioned that the numbers of hidden neurons are often determined by a trial-and-error procedure.

The trend of the calculation process in this model is written in Eq. 3. The learning algorithm formula in the MLP model is written in Eq. (4). η is the learning rate, a small positive value that controls the adjustment magnitude. y_{true} is the actual value. y_{predict} is the predicted value. Also, w_{i+1} and w_i refer to the new and old values of the weights, respectively.

$$Y = f_2 \left(\sum_{i=1}^n w_j \times f_1 \left(\sum h_{ij} x_i + b_j \right) + b_o \right) \quad (3)$$

$$w_{i+1} = w_i + \eta \times (y_{\text{true}} - y_{\text{predict}}) \times x_i \quad (4)$$

The symbols of ' h_{ij} ', ' b_j ', ' f_1 ' are the weights vector, biases, and activation function in the hidden layer, and ' w_j ', ' b_o ', ' f_2 ' are the weights vector, biases, and activation function in the output layer.

RBF network

This ANN type has Gaussian and linear functions in the hidden and output portions, respectively. Equations (5) and (6) show the mathematical formula of Gaussian and linear activation functions, respectively⁴⁴.

$$f(\text{net}) = e^{-\frac{\text{net}^2}{2\sigma^2}} \quad (5)$$

$$f(\text{net}) = \text{net} \quad (6)$$

where σ refers to the spread of the Gaussian relation.

Statistical analysis

Several statistical criteria are employed to monitor the performance of the developed RBF and MLP. Equations (9) to (12) show the mathematical expressions of different kinds of errors, and the correlation coefficient, respectively^{45,46}.

$$\text{AARD\%} = \frac{100}{N} \sum_n^N \frac{|S_n^{\text{act}} - S_n^{\text{pred}}|}{S_n^{\text{act}}} \quad (7)$$

$$\text{MSE} = \frac{1}{N} \sum_{n=1}^N (S_n^{\text{act}} - S_n^{\text{pred}})^2 \quad (8)$$

$$\text{RMSE} = \left(\frac{1}{N} \sum_{n=1}^N (S_n^{\text{act}} - S_n^{\text{pred}})^2 \right)^{0.5} \quad (9)$$

$$R^2 = 1 - \frac{\sum_{n=1}^N (S_n^{\text{act}} - S_n^{\text{pred}})^2}{\sum_{n=1}^N (S_n^{\text{act}} - \bar{S}^{\text{pred}})^2} \quad (10)$$

wherein 'S' shows CO₂ mole fraction in [Bmim][PF₆], and 'N' refers to the number of available data.

Results and discussion

This study aims to detect the suitable topology of the MLP and RBF networks, compare their predictive performances, and find the most accurate model to estimate CO₂ solubility in [Bmim][PF₆] ionic liquid. Therefore, the next three sections are devoted to RBF model design, MLP development, and a comparison of their results to find the most accurate model. The more precise model is validated using the collected experimental database. Finally, the proposed model is applied to probe the impact of temperature and pressure on the CO₂ mole fraction in [Bmim][PF₆].

RBF model developing

During any RBF neural network development, it is essential to find the number of hidden neurons and the spread value (for the Gaussian transfer function of the hidden layer). The minimum number of hidden neurons equals one, while its maximum number is often determined using a rule of thumb⁴⁷. The number of training datasets should be 2–10 times the number of adjustable parameters, like weights and biases of the ANN model^{48–54}. In this work, the middle value of this range (i.e., six) is utilized to detect the maximum quantity value of hidden neurons. Our experimental datasets (371 data points) are accidentally classified into training and testing subdivisions (75%:25%). Indeed, we have 278 training and 93 testing datasets. The RBF neural network with two independent variables, K hidden neurons, and one dependent variable poses 4 K + 1 weights and biases. Therefore, available training datasets should be higher than 6 × (4 K + 1). It can be simply concluded that the maximum number of hidden neurons is eleven. Therefore, various RBF neural networks differing in the number of hidden neurons and spread value are designed. For the RBF model with one to eleven hidden neurons, the spread values of 0.0001 to 10 are used. Indeed, 1100 RBF neural networks are developed during this analysis. Figure 1 presents the most accurate results obtained by the RBF model with various numbers of hidden neurons.

The RBF neural network's principle states that this model automatically adds one hidden neuron for each training dataset. Therefore, it is necessary to develop RBF neural networks with more than eleven hidden neurons and monitor their predictive performances. Several new RBF neural networks (with 12 to 278 hidden neurons) with different spread values are developed in this stage, and their accuracy during the training and testing stages is measured. The most accurate results obtained by different RBF structures are summarized in Table S1. It can be observed that the RBF model with the 2-42-1 architecture and spread = 0.1353 presented the most suitable accuracy for predicting CO₂ mole fraction in the [Bmim][PF₆]. It is worth noting that constructing the RBF model with more than 42 hidden neurons results in network overfitting.

To provide the readers with a visual observation of the overfitting concept, the accuracy of the RBF network with a 2-278-1 structure is presented. Figure 1 illustrates the performance of this RBF neural network for training, testing, and overall datasets. It can be seen that the RBF model with the small spread value shows excellent accuracy for the training datasets, but its performance for the testing subdivision is entirely unacceptable. It can be concluded that using the small spread value results in overfitting the RBF neural networks with 278 hidden neurons. In summary, the RBF neural networks with 278 hidden neurons and spread values higher than one show relatively similar performances (AARD ≈ 0.6%). Comparing the reported results in Figs. 1 and 2 confirmed that increasing the number of hidden neurons of the RBF neural networks produces no significant improvement in accuracy. Indeed, the RBF model with ten hidden neurons presents better results than the RBF model with 278 hidden neurons.

MLP model development

The number of hidden neurons, transfer functions of hidden and output layers, and training algorithm need to be determined for the MLP model. Like the RBF, the maximum value of hidden neurons for the MLP is eleven. Four different combinations of the tangent and logarithm sigmoid have been utilized as transfer functions in the MLP neural networks in this work. Moreover, nine different optimization algorithms are employed to train the MLP models. More specifically, we developed 7920 MLP neural networks (11 × 4 × 9 × 20) (numbers of hidden neurons × four combinations of transfer function × nine training algorithms × twenty tries per structure) in

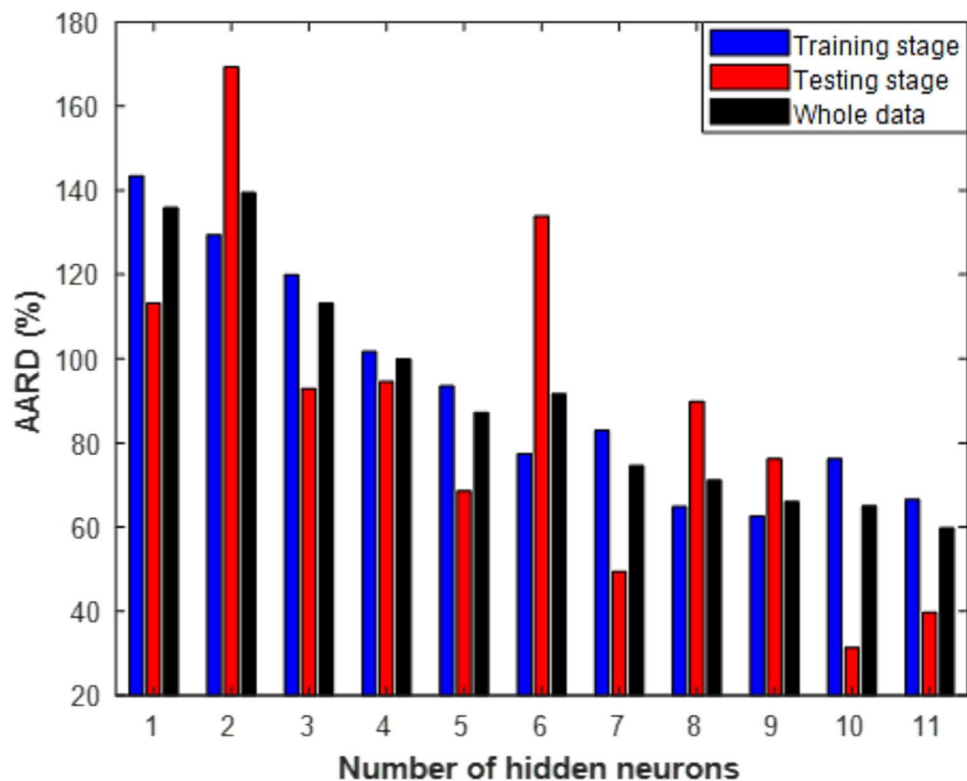


Fig. 1. The best-obtained results by the RBF neural network with different numbers of hidden neurons.

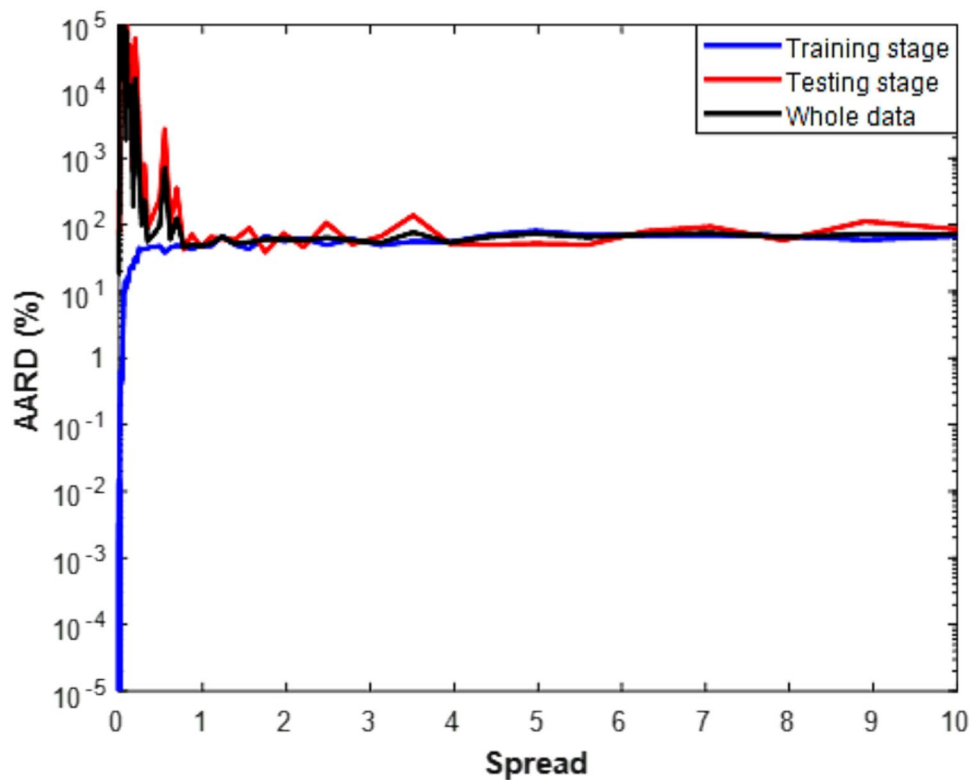


Fig. 2. Presented relative deviation by the RBF models with 278 hidden neurons and different spread values.

this study. Table S2 summarizes the most accurate results obtained by different structures of the MLP neural networks.

The reported results in Table S2 confirmed that a network with eleven hidden neurons, tangent and logarithm sigmoid transfer functions in hidden and output layers, trained by the Levenberg–Marquardt algorithm, is the best MLP model among the 7920 designed paradigms.

Suitable ANN model selection

Figure 3 schematically explains a procedure used in this study to find the most suitable model. Concisely, a comparison between the best RBF and MLP models' accuracy shows that the latter is the most suitable approach for anticipating the CO₂ mole fraction in the [Bmim][PF₆] ionic liquid.

Here, the AARD index is only used to monitor the accuracy of the developed smart models. There exist some other statistical indices that are often employed to measure the accuracy of a model. Table 3 reports the accuracy of the best-designed MLP and RBF neural networks in terms of performance parameters for training, testing, and the whole databank.

The structure of the developed MLP neural network is presented in Fig. 4. As mentioned earlier, temperature and pressure are independent variables, and CO₂ solubility in [Bmim][PF₆] ionic liquid is considered a dependent variable. Moreover, this model has the structure of 2-11-1, tangent sigmoid, and logarithmic sigmoid transfer functions in hidden and output layers, respectively. Furthermore, the Levenberg–Marquardt optimization technique is the best training algorithm for adjusting the MLP model hyperparameters. Figure 5 shows that the training algorithm continuously decreases the observed error up to 600 iterations, and the training stage is finished.

Values of weights and biases of the trained MLP model by the Levenberg–Marquardt are presented in Table 4. This type of information is required to use our developed MLP model by others. The reported weights and biases in this table, along with the activation functions, are the only information that needs to be used in our MLP neural network for estimating CO₂ mole fraction.

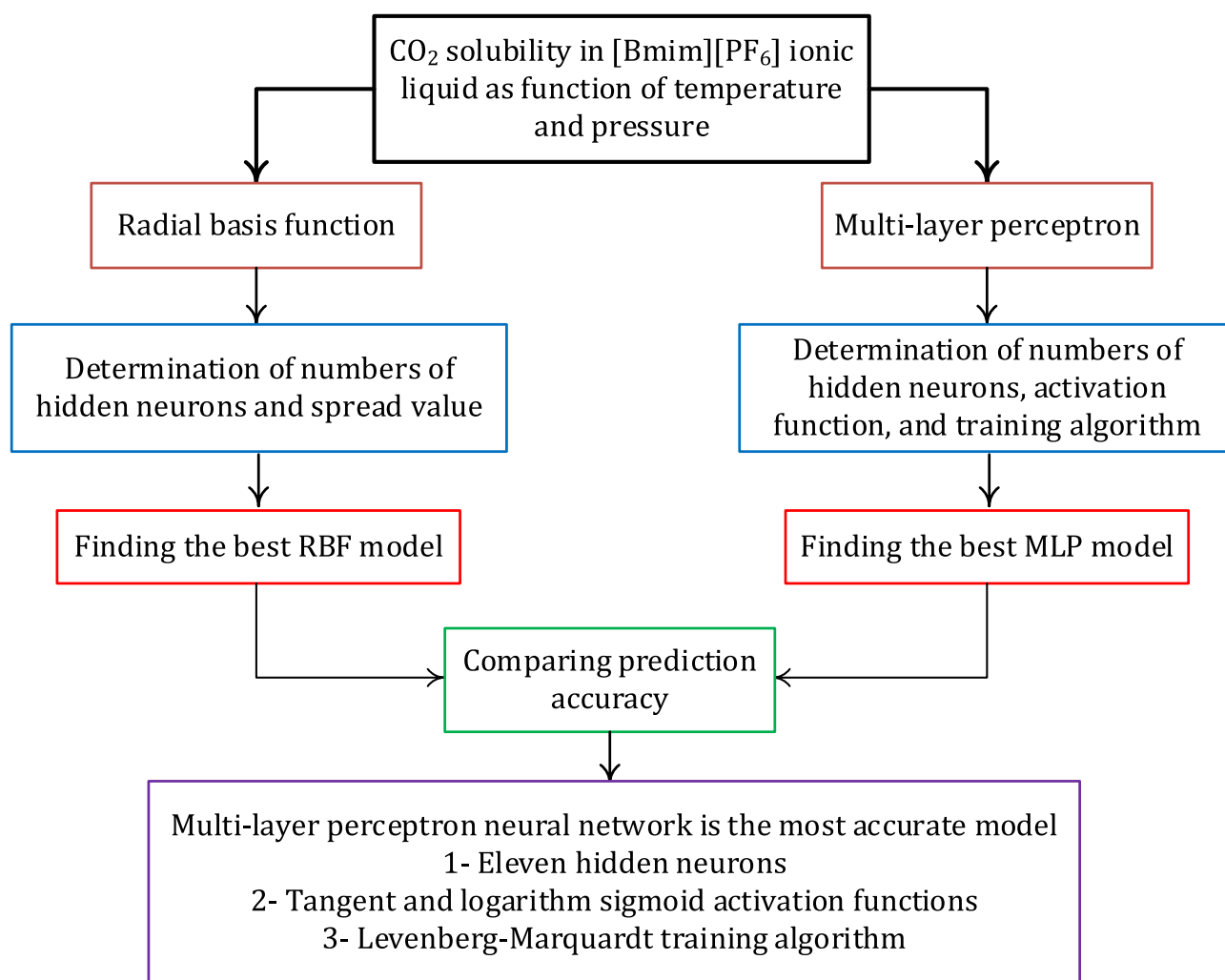


Fig. 3. The employed procedure to find the most accurate paradigm for predicting CO₂ mole fraction in the [Bmim][PF₆].

ANN model	Topology	Database	Four well-known statistical indices			
			AARD%	MSE	RMSE	R ²
MLP	2-11-1	Training	0.02355	0.0021	0.046	0.9709
		Testing	0.02759	0.0022	0.047	0.9791
		Whole data	0.02456	0.0021	0.046	0.9734
RBF	2-42-1	Training	0.03370	0.0034	0.058	0.9576
		Testing	0.03204	0.0073	0.085	0.9081
		Whole data	0.03328	0.0043	0.066	0.9449

Table 3. Measurement of the accuracy of the designed best MLP and RBF models using four well-known statistical criteria.

Proposed MLP validation

The focus of this section is devoted to the validation of the most accurate MLP model using experimental data. For this purpose, a graphical presentation based on the cross-plot is used. Cross-plot is a well-known method to check the performance of a model. It presents the predicted values as a function of their corresponding actual data points. The diagonal line of the cross-plot shows the exact adaptation of the predictions to their corresponding actual values. Figure 6 illustrates the cross-plot of predicted CO₂ solubility versus the actual information for the training stage. It can be seen that major parts of the red circle symbols are almost concentrated around the diagonal line.

The Leverage analysis of the MLP model was conducted, and its related regression plots are shown in Fig. 7 for the purpose of validating the MLP model with the experimental results. The Leverage approach was used for the MLP model because this model has better performance than the RBF model. According to Fig. 7, the regression coefficient in the validation of experimental results with the predicted data is 0.96269, indicating a good adaptation between the MLP model and the experimental results.

The cross-plot for the whole of the datasets (training + testing) is presented in Fig. 8. Figures 6 and 9 also confirmed the moderate behavior of the MLP network for anticipating the experimental database of CO₂ solubility in the [Bmim][PF₆] ionic liquid.

It was mentioned previously that so collected the experimental database was collected from thirteen different research studies. We think it is good to monitor the performance of the designed MLP neural network to predict the reported datasets in the various manuscripts. Figure 10 presents the efficiency of the developed MLP paradigm in terms of deviation percentage for predicting experimental datasets reported in different references. It is clear that the MLP neural network explains the worst results in predicting the experimental data reported by Afzal et al.³⁸. The next highest deviation percentage are devoted to the reported datasets by Yokozeki et al.³³ and Shiflett and Yokozeki⁴², respectively. Our developed MLP approach predicted the experimental measurements in these references with the deviation of 53% and 34%, respectively. Experimental datasets about CO₂ solubility in [Bmim][PF₆] in all other references are predicted with an deviation of less than 28%. On the other hand, the MLP neural network predicted the experimental measurements by Kodama et al.³⁹ with the highest accuracy, i.e., deviation percentage of 8.27%. It is noteworthy that the value of deviation percentage in this current work has been calculated at 0.02456% which is lower than the other works mentioned above. It is noteworthy that the value of deviation percentage in this current work has been calculated at 0.02456% which is lower than the other works mentioned above, and proves that the ANN structure for this work is better than the other works mentioned above.

Effect of temperature and pressure

The effect of isothermal change in pressure on CO₂ solubility in 1-N-butyl-3-methylimidazolium hexafluorophosphate ionic liquid is displayed in Fig. 7. Figure 11 presents experimental data as well as their corresponding predictions by the MLP model. It is obvious that the MLP paradigm correctly predicts the trend of CO₂ solubility in [Bmim][PF₆] versus isothermal change in pressure. It is worth noting that the MLP model provides the AARD of 0.0859%, 0.00874%, and 0.03088% for temperatures of 283.15, 298.15, and 323.15 K, respectively. These observed deviations confirmed that the MLP neural network presents higher inaccuracy for predicting CO₂ solubility at higher temperatures. This may be associated with the smaller number of available experimental datasets for higher temperatures. Moreover, both experimental data and MLP results proved that the CO₂ mole fraction in [Bmim][PF₆] increases by isothermal enhancing of the operating pressure. This observation is in agreement with the fact that the CO₂ mole fraction in liquids increases with increasing pressure.

Variation of CO₂ solubility in the given ionic liquid as a function of isobar change of temperature from the experimental and predicted values is presented in Fig. 12. This figure shows a relatively good agreement between actual data points and MLP predictions. Our MLP model correctly detects the profile of CO₂ solubility versus isobaric change of temperature. On the other hand, experimental and modeling results confirmed that increasing temperature decreases the CO₂ mole fraction in the [Bmim][PF₆]. The results are also in agreement with the scientific fact that gas solubility in liquids decreases with increasing temperature.

For describing the CO₂ solubility mechanism in the ionic liquid, equations that relate Henry's constant (H_{CO_2}) to the pressure and temperature can be helpful. Carroll et al.⁵⁵ explain the dependency of CO₂ solubility on the Henry's constant on temperature and pressure. Equation (11) is the dependency of CO₂ solubility on the Henry's constant at different pressures. Equation (12) is the dependency of CO₂ solubility on the Henry's

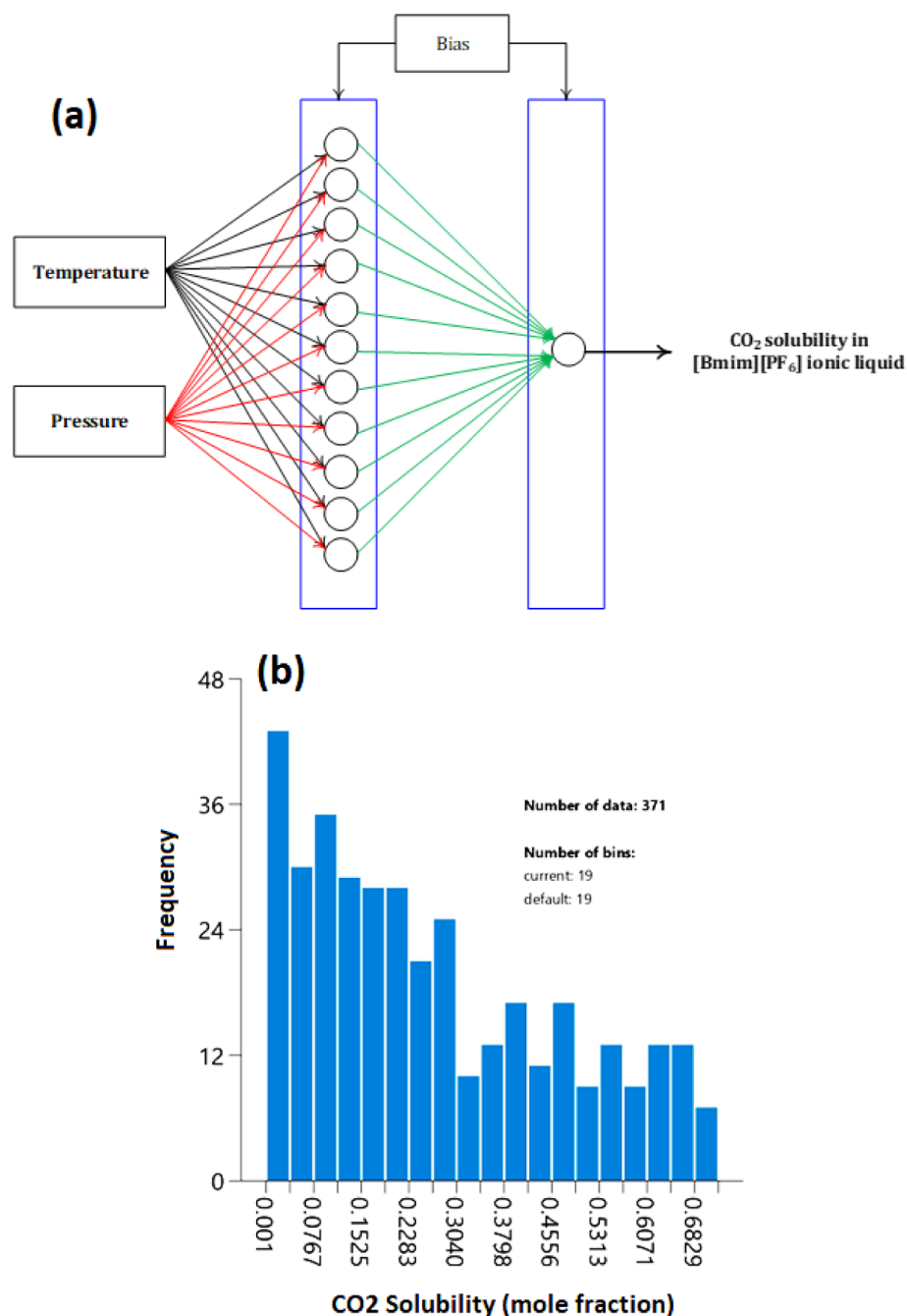


Fig. 4. (a) The best MLP structure for prediction of the CO₂ mole fraction in [Bmim][PF₆], (b) The histogram diagram of the experimental data.

constant at different temperatures. According to Eq. (11), pressure increase leads to an increase in the CO₂ solubility. Indeed, Pressure increase can increase the Henry's constant. Besides, pressure increase causes a change in Henry's constant, and finally a change in the CO₂ solubility. Equation (12) also proved that the temperature increase leads to an elevation of Henry's constant, which means a positive influence on the CO₂ solubility in the ionic liquid. This conclusion was also observed in the work of Carroll et al. In our work, the ANN predicts that the temperature (Fig. 12) and pressure (Fig. 11) increase lead to CO₂ solubility elevation in the ionic liquid, which is owing to the increase the Henry's constant.

$$P_{\text{CO}_2} = H_{\text{CO}_2} \cdot x_{\text{CO}_2} \quad (11)$$

$$\ln H_{\text{CO}_2} = -6.8346 + \frac{1.2817 \times 10^4}{T} - \frac{3.7668 \times 10^6}{T^2} + \frac{2.997 \times 10^8}{T^3} \quad (12)$$

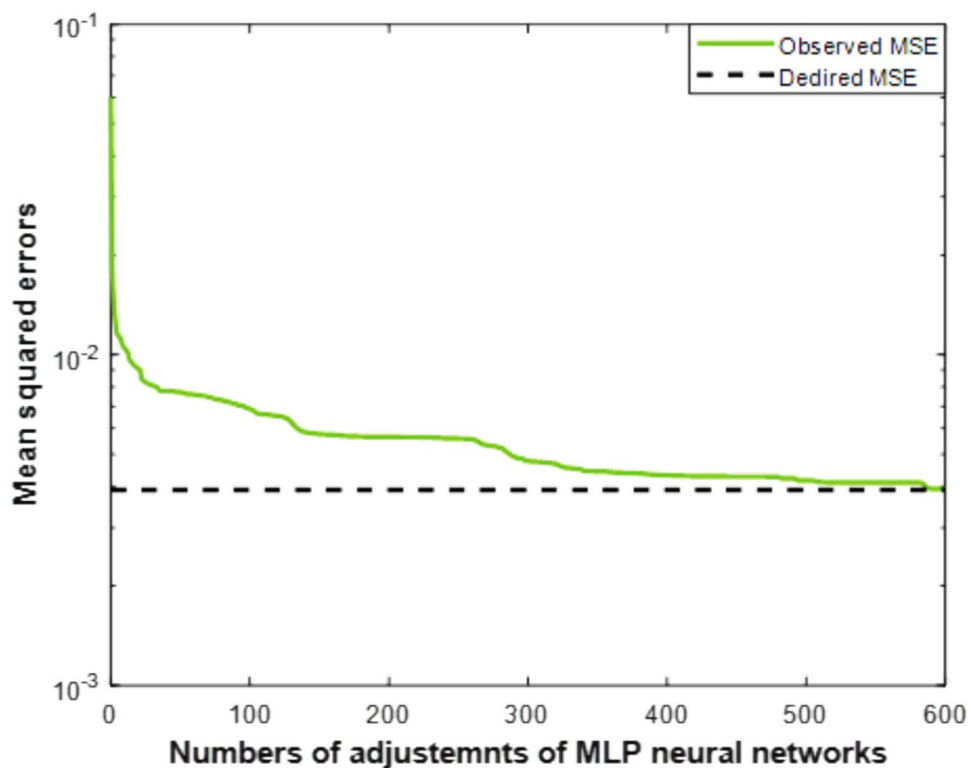


Fig. 5. Variation of the mean square error of the proposed MLP model during training by the Levenberg–Marquardt algorithm.

Hidden Neuron	First neuron layer			Second neuron layer	
	Weight matrix			Weight vector	Bias
	Temperature	Pressure	Bias vector		
1	-1.0586	-2.1805	-0.42108	-1.2246	-24.1089
2	0.78276	-27.8142	-28.2085	-23.4109	
3	0.85932	30.2653	25.8187	-28.2463	
4	-0.73747	-31.3756	-26.65	-27.6581	
5	4.7153	0.031223	2.1689	13.3708	
6	-52.8136	-4.1687	-30.3598	-2.5653	
7	-372.921	-92.3877	-311.175	0.56877	
8	3.2319	0.085459	2.1581	-37.69	
9	48.4915	1.4673	33.7003	3.116	
10	-3.6256	-0.92998	-3.8036	-16.568	
11	23.1182	-2.9099	15.544	2.4734	

Table 4. Weights and biases of the proposed MLP model.

The van't Hoff formula is written in Eq. (13). The van't Hoff formula relates the thermodynamic equilibrium constant (K) to the temperature. The values of enthalpy change (ΔH) and entropy change (ΔS) can be calculated with this formula. The graph of $\ln(K)$ vs T^{-1} was plotted in Fig. 13. The slope and intercept of Fig. 13 are $-\frac{\Delta H^\circ}{R}$ and $\frac{\Delta S^\circ}{R}$, respectively. The values of enthalpy change and entropy change were determined at $22.802 \text{ kJ} \cdot \text{mol}^{-1}$ and $0.0703 \text{ kJ} \cdot \text{mol}^{-1} \cdot \text{K}^{-1}$, respectively. It was concluded that the absorption of CO_2 molecules with [Bmim][PF₆] is endothermic with an irregular pattern, because of the positive sign of the enthalpy change and also the entropy change, respectively.

$$\ln(K) = \left(-\frac{\Delta H^\circ}{R} \right) \cdot \frac{1}{T} + \frac{\Delta S^\circ}{R} \quad (13)$$

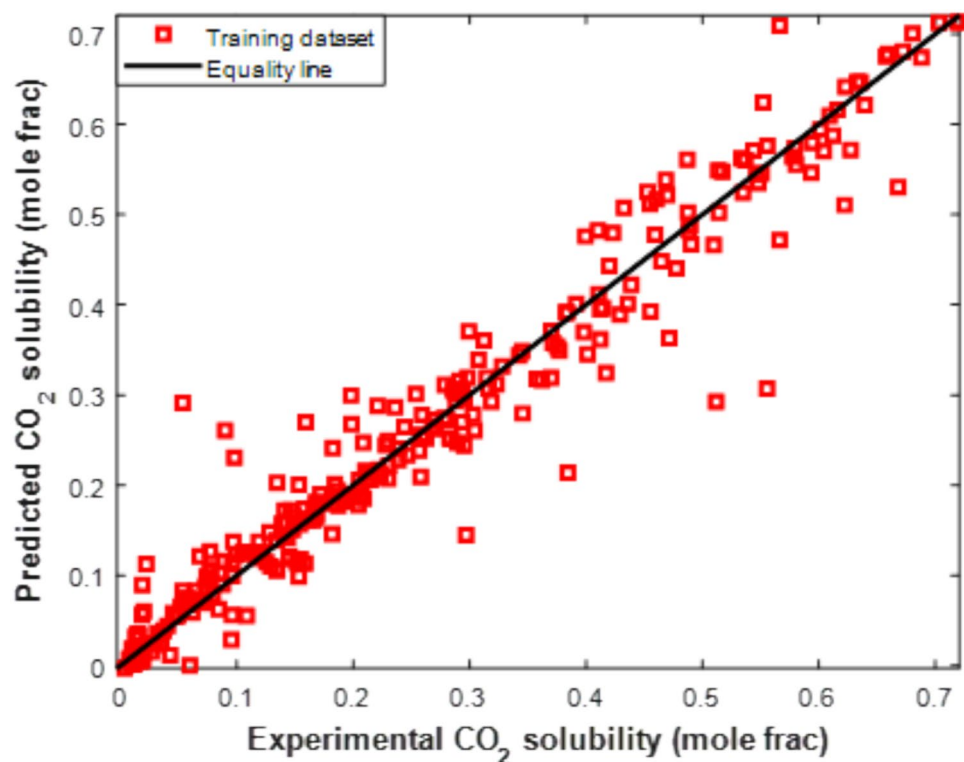


Fig. 6. Cross-plot of predicted versus experimental CO₂ solubility during the training stage.

Simultaneous parameter effect

In this section, the effect of simultaneous changes in temperature and pressure on CO₂ solubility in 1-N-butyl-3-methylimidazolium hexafluorophosphate ionic liquid is simulated using the proposed MLP model (Fig. 14). It is observed from Fig. 14 that the CO₂ mole fraction in the [Bmim][PF₆] increases by enhancing pressure and decreasing temperature. Actually, the maximum CO₂ mole fraction in the given ionic liquid is achieved at the highest pressure and lowest temperature (i.e., pressure of 200 bar and temperature of 283 K). The fluctuations that appeared in this figure may be associated with the uncertainty in the MLP predictions, which was about 0.025% in terms of relative deviation.

Future recommendations

Some recommendations about the ANN method in the field of CO₂ capture can be useful for scientists working in the future. In our opinion, scientists can consider ionic liquids, eutectic solvents, and organic solvents as inputs. Additionally, other variables, such as activity coefficient, fugacity coefficient, acentric factor, and additives, can be defined as inputs. Other separation tools, like adsorbents, can be added to the other inputs, like ionic liquids, for detecting a better option for CO₂ capture. Moreover, other outputs, such as absorption efficiency, can also be studied in addition to CO₂ solubility. The other recommendation is entering data with the use of Aspen Plus and molecular dynamics (MD) because of a lack of enough experimental data. It is recommended to apply other ANN methods, like SVM, to study the CO₂ solubility in [Bmim][PF₆] ionic liquid. One of the challenges in the ANN method is entering a high amount of data as inputs, which can be solved by experts in the fields of computer engineering and chemical engineering.

Conclusions

CO₂ solubility in [Bmim][PF₆] is modeled using MLP and RBF. The MLP model predicted 371 experimental datasets with the least error and the highest adaptation to the experimental data. The structure of the suggested MLP model has eleven hidden neurons, tangent and logarithm sigmoid in hidden and output layers, and trained by the Levenberg–Marquardt algorithm. Also, the results confirmed that the MLP neural network presents higher inaccuracy for predicting CO₂ solubility at higher temperatures. Sensitivity analysis on the RBF neural network structure showed that increasing the number of hidden neurons to more than 10 has no positive effect on its accuracy. It is recommended that the other neural networks be used in future work. Also, it is interesting to define more than one ionic liquid as input in an ANN to determine the better ionic liquid for CO₂ elimination.

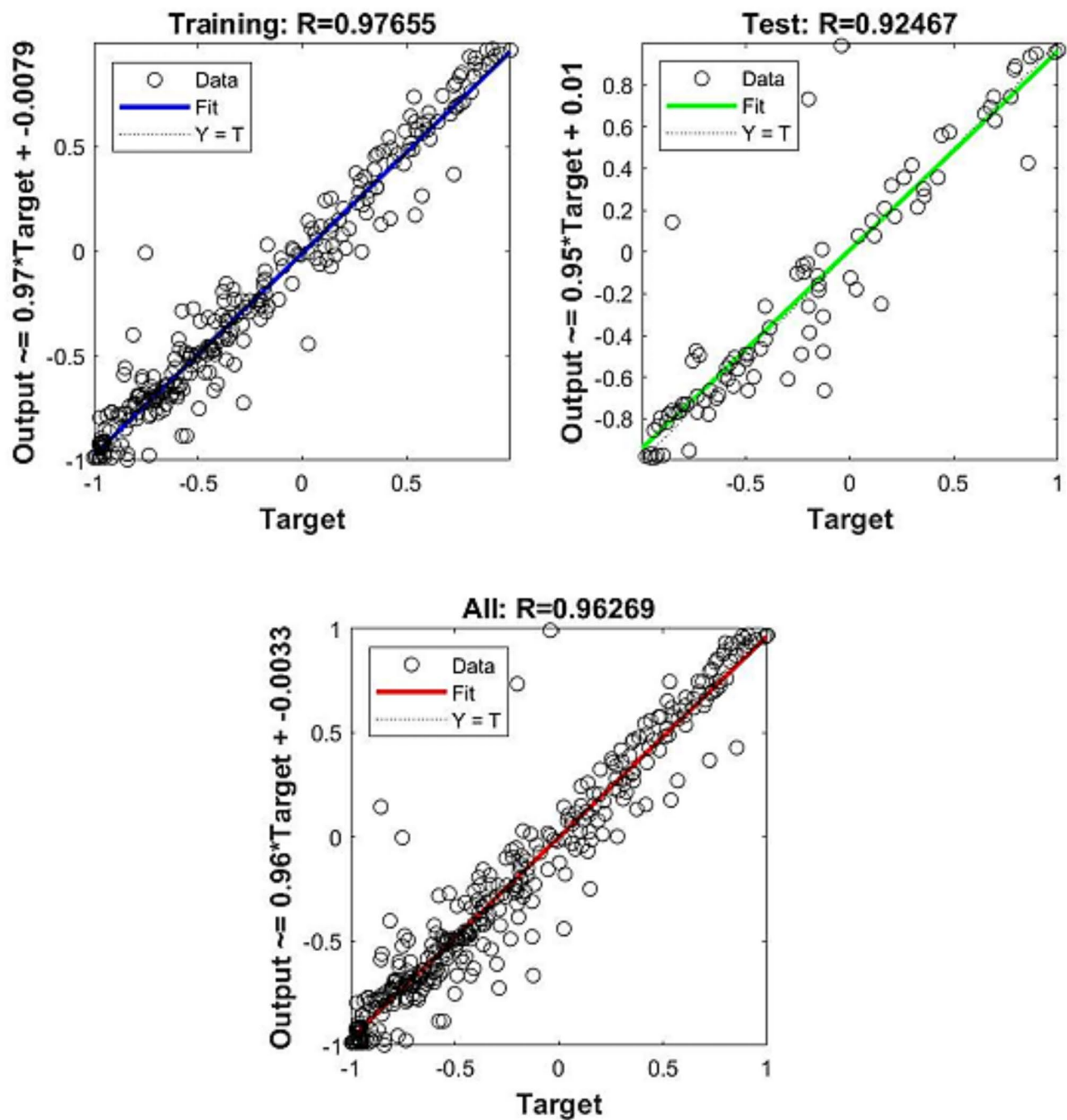


Fig. 7. The Leverage analysis for studying the validation process in the MLP model.

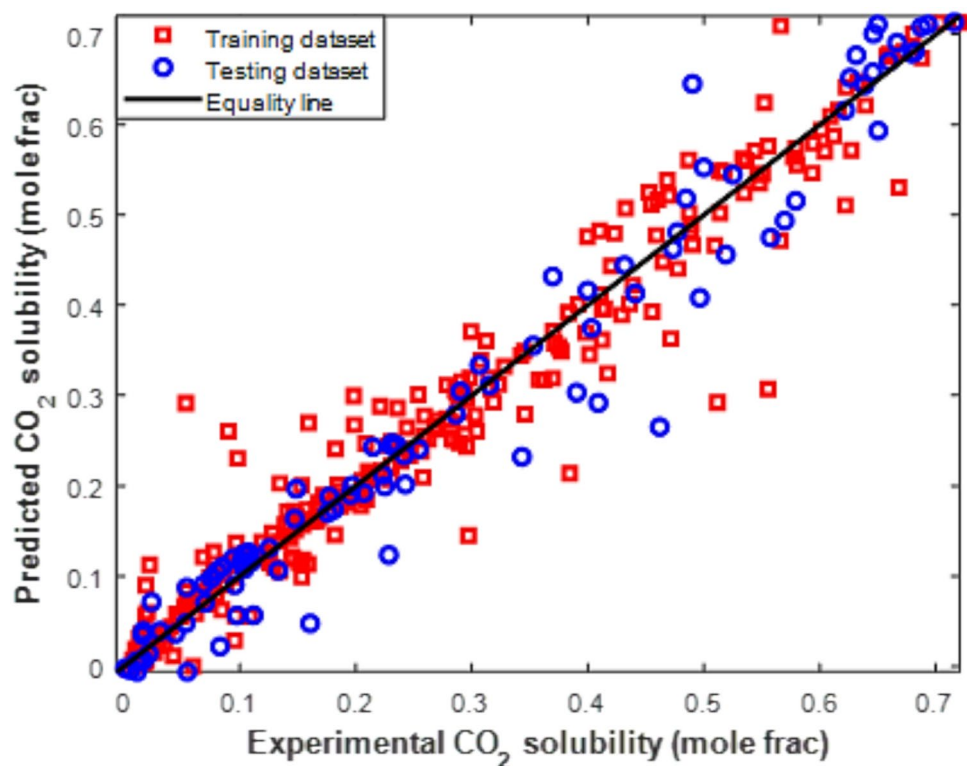


Fig. 8. Performance of the MLP network for the prediction of the 371 experimental data for the CO₂ mole fraction.

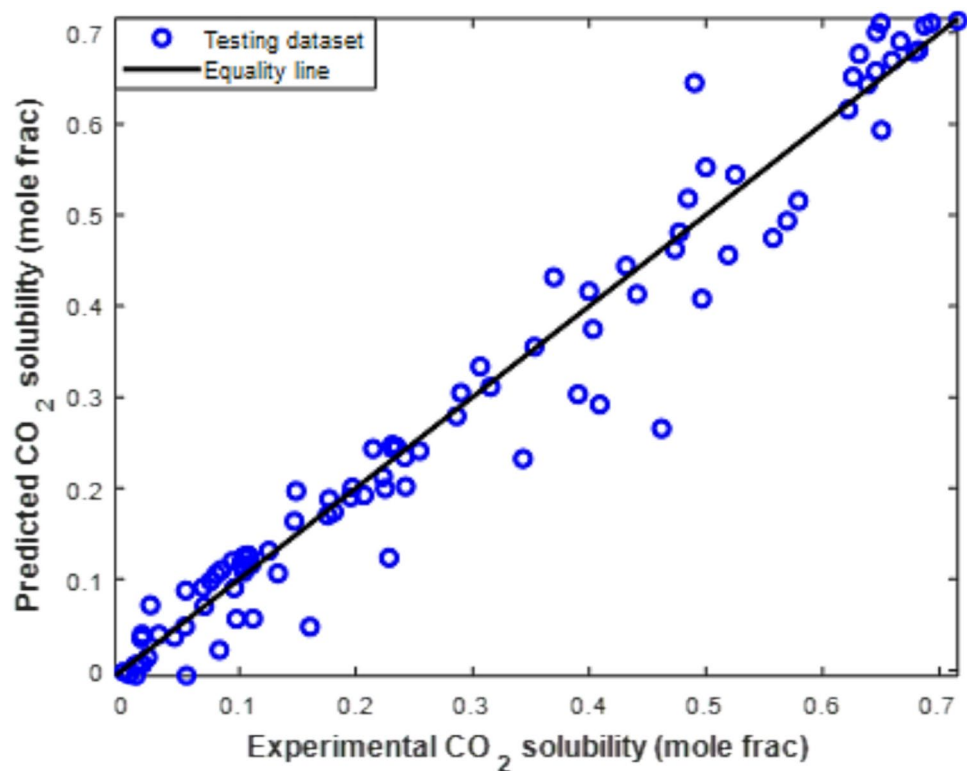


Fig. 9. The MLP predictions versus their associated experimental values for the testing subdivision.

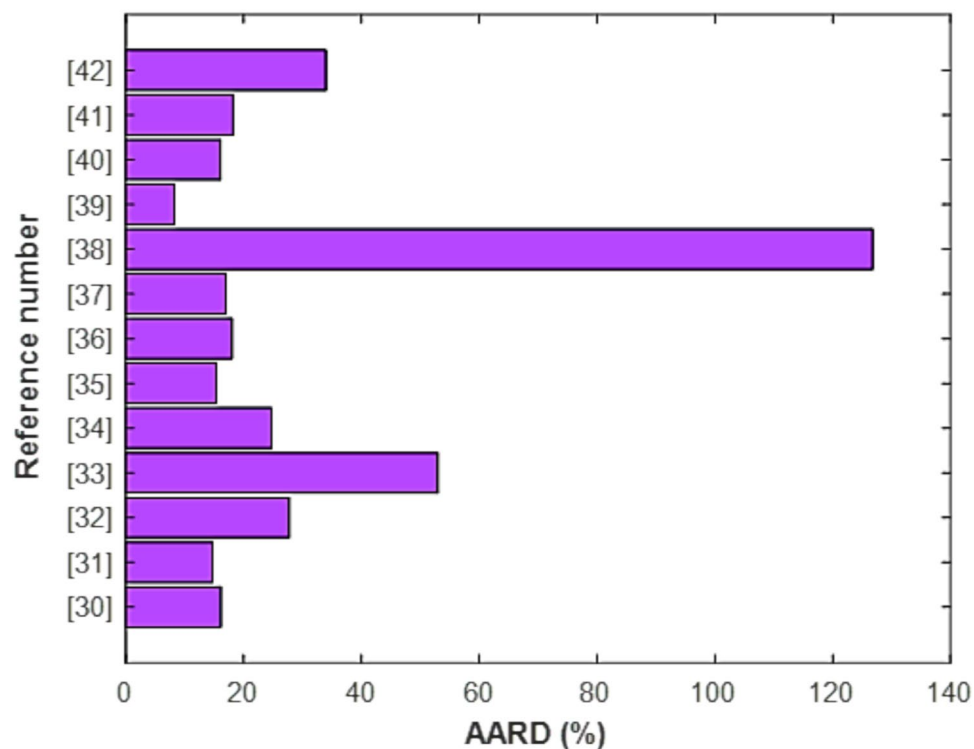


Fig. 10. Performance of the MLP neural network for estimating experimental datasets reported by different researchers.

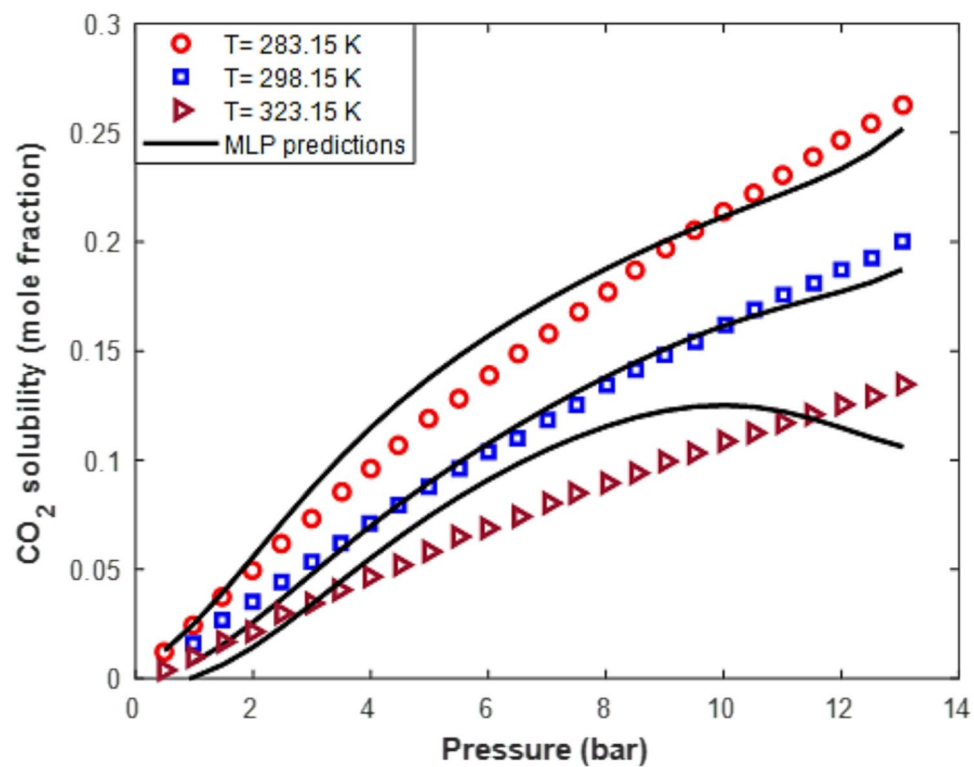


Fig. 11. Difference of CO₂ mole fraction in the [Bmim][PF₆] with isothermal enhancing of the pressure.

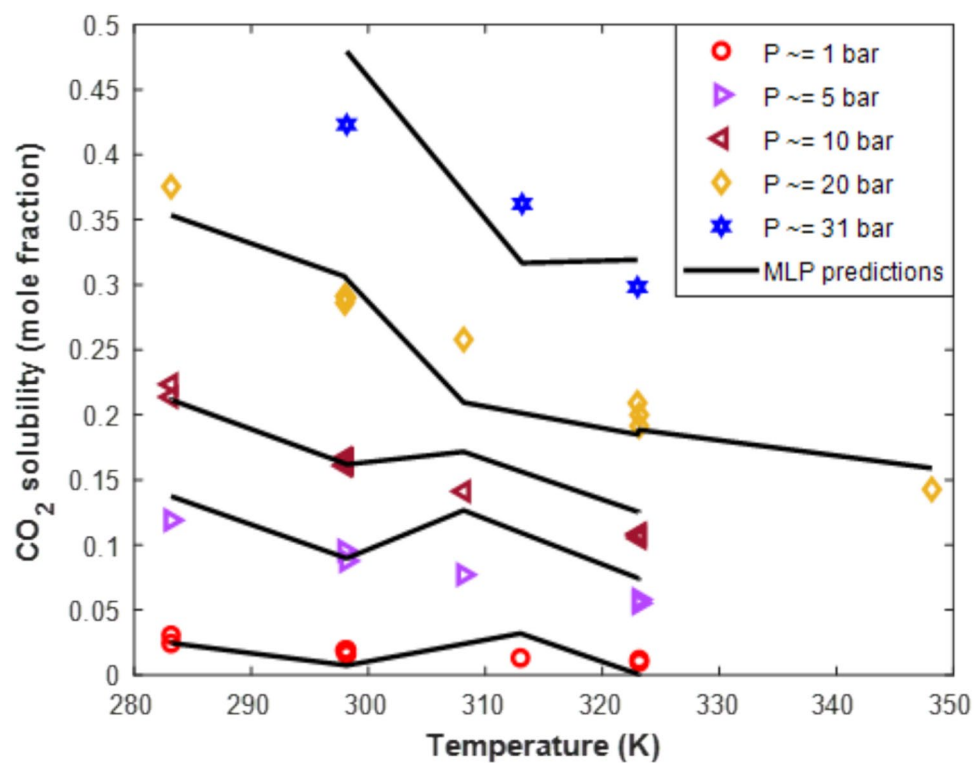


Fig. 12. The effect of the isobaric increase in the temperature on the CO₂ solubility in the [Bmim][PF₆] ionic liquid.

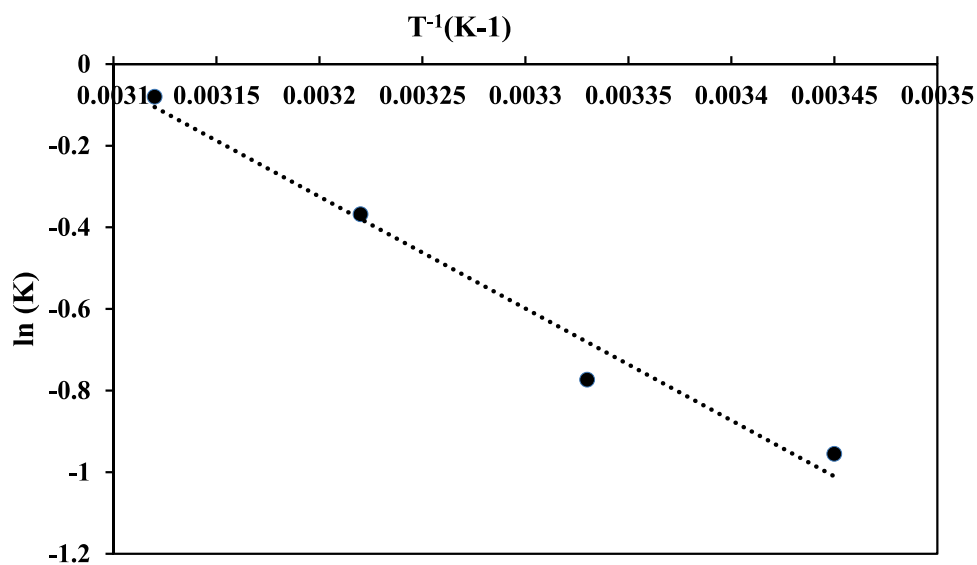


Fig. 13. The plot of ln(K) vs T⁻¹.

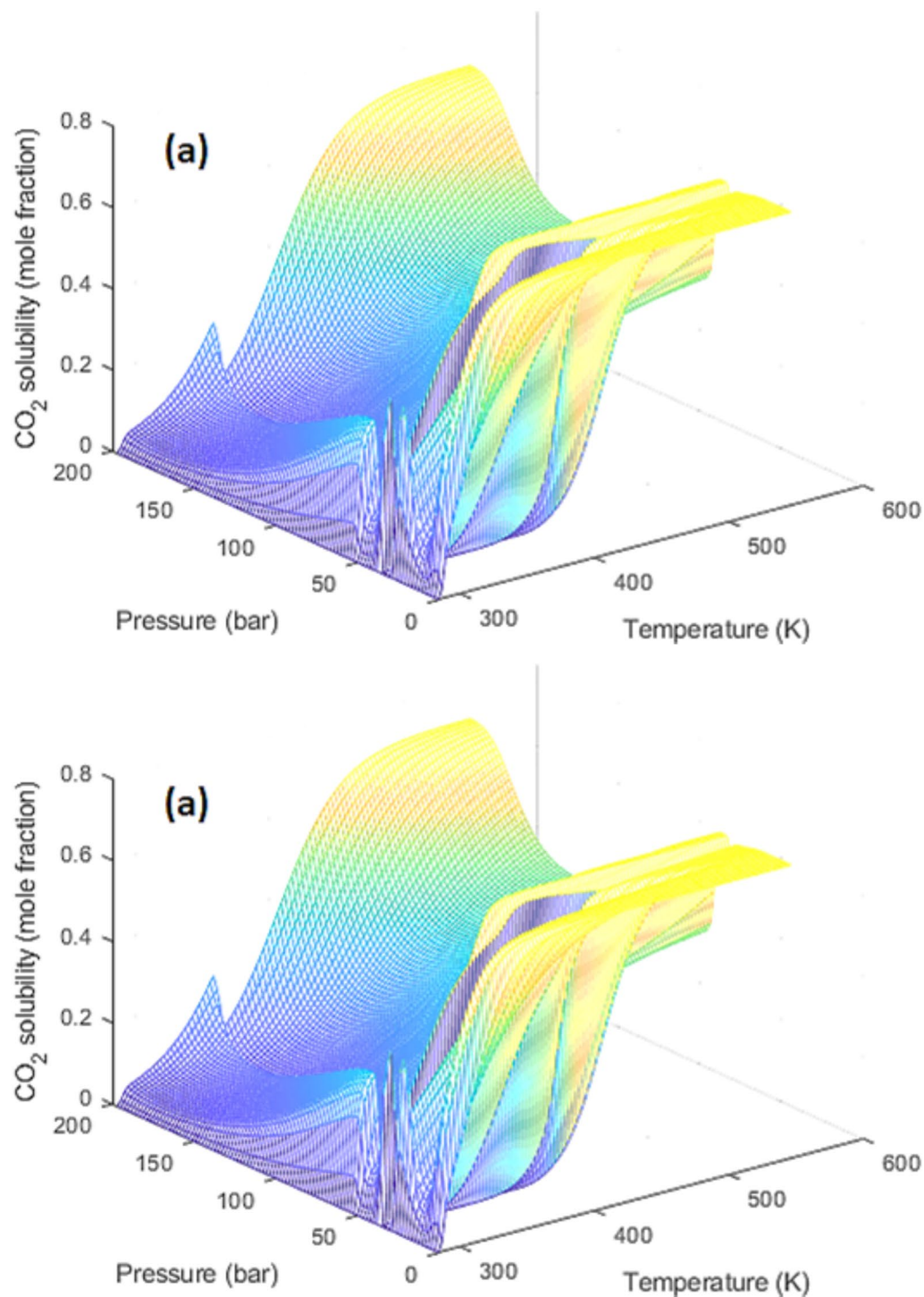


Fig. 14. Three-dimensional simulation graph for the effect of pressure and temperature on CO₂ mole fraction in [Bmim][PF₆] for (a) MLP model (train function: trainlm, transfer function for first layer: tansig, transfer function for second layer: logsig), (b) MLP model (train function: traincgb, transfer function for first layer: tansig, transfer function for second layer: tansig).

Data availability

The datasets used and/or analysed during the current study available from the corresponding author on reasonable request.

Received: 13 September 2025; Accepted: 2 December 2025

Published online: 03 December 2025

References

- Anderson, T. R., Hawkins, E. & Jones, P. D. CO₂, the greenhouse effect and global warming: from the pioneering work of Arrhenius and Callendar to today's Earth System Models. *Endeavour* **40**(3), 178–187 (2016).
- Kohl, A. L. Alkanolamines for hydrogen sulfide and carbon dioxide removal. *Gas Purific.* **1985**, 29–35 (1985).
- Spratt, D. & Sutton, P. *Climate Code Red* (David Spratt, 2008).
- Dashti, A. et al. Evaluation of CO₂ absorption by amino acid salt aqueous solution using hybrid soft computing methods. *ACS Omega* **6**(19), 12459–12469 (2021).
- Amirkhani, F. et al. Estimation of CO₂ solubility in aqueous solutions of commonly used blended amines: application to optimised greenhouse gas capture. *J. Clean. Prod.* **430**, 139435 (2023).
- Amirkhani, F. et al. Estimation of CO₂ absorption by a hybrid aqueous solution of amino acid salt with amine. *Chem. Eng. Technol.* **47**(2), 253–261 (2024).
- Alatefi, S. et al. Explainable artificial intelligence models for estimating the heat capacity of deep eutectic solvents. *Fuel* **394**, 135073 (2025).
- Alatefi, S. et al. Toward explicit learning frameworks for predicting the solubility of CO₂–N₂ gas mixtures in brine: implications for impure CO₂ storage in saline aquifers. *J. Contam. Hydrol.* **2025**, 104660 (2025).
- Amirkhani, F. et al. Towards estimating absorption of major air pollutant gasses in ionic liquids using soft computing methods. *J. Taiwan Inst. Chem. Eng.* **127**, 109–118 (2021).
- Hiraga, Y. et al. Measurement and modeling of CO₂ solubility in [bmim] Cl–[bmim][Tf₂N] mixed-ionic liquids for design of versatile reaction solvents. *J. Supercrit. Fluids* **132**, 42–50 (2018).
- Yim, J.-H., Ha, S.-J. & Lim, J. S. Measurement and correlation of CO₂ solubility in 1-butyl-3-methylimidazolium ([BMIM]) cation-based ionic liquids:[BMIM][Ac],[BMIM][Cl],[BMIM][MeSO₄]. *J. Supercrit. Fluids* **138**, 73–81 (2018).
- Altamash, T. et al. Carbon dioxide solubility in phosphonium-, ammonium-, sulfonyle-, and pyrrolidinium-based ionic liquids and their mixtures at moderate pressures up to 10 bar. *J. Chem. Eng. Data* **62**(4), 1310–1317 (2017).
- Zhao, Z. et al. Experiment and simulation study of CO₂ solubility in dimethyl carbonate, 1-octyl-3-methylimidazolium tetrafluoroborate and their mixtures. *Energy* **143**, 35–42 (2018).
- Hoga, H. E., Olivieri, G. V. & Torres, R. B. Experimental measurements of volumetric and acoustic properties of binary mixtures of 1-Butyl-3-methylimidazolium hexafluorophosphate with molecular solvents. *J. Chem. Eng. Data* **65**(7), 3406–3419 (2020).
- Alatefi, S. et al. Accurate prediction of water activity in ionic liquid-based aqueous ternary solutions using advanced explainable artificial intelligence frameworks. *Chem. Eng. Sci.* **318**, 122218 (2025).
- Amirkhani, F. et al. Modeling and estimation of CO₂ capture by porous liquids through machine learning. *Sep. Purif. Technol.* **359**, 130445 (2025).
- Khosrafiar, Z. & Ghaemi, A. Prediction of CO₂ solubility in water at high pressure and temperature via deep learning and response surface methodology. *Case Stud. Chem. Environ. Eng.* **7**, 100338 (2023).
- Hasanzadeh, A., Ghaemi, A. & Shahhosseini, S. Neural network modeling for development of high-pressure measurement of carbon dioxide solubility in the aqueous AEEA+ sulfolane. *J. Chem. Petrol. Eng.* **57**(2), 179–197 (2023).
- Eslamimanesh, A. et al. Artificial neural network modeling of solubility of supercritical carbon dioxide in 24 commonly used ionic liquids. *Chem. Eng. Sci.* **66**(13), 3039–3044 (2011).
- Gholizadeh, F. & Sabzi, F. Prediction of CO₂ sorption in poly (ionic liquid) s using ANN-GC and ANFIS-GC models. *Int. J. Greenhouse Gas Control* **63**, 95–106 (2017).
- Baghban, A., Ahmadi, M. A. & Shahraki, B. H. Prediction carbon dioxide solubility in presence of various ionic liquids using computational intelligence approaches. *J. Supercrit. Fluids* **98**, 50–64 (2015).
- Venkatraman, V. & Alsberg, B. K. Predicting CO₂ capture of ionic liquids using machine learning. *J. CO₂ Utiliz.* **21**, 162–168 (2017).
- Tatar, A. et al. Prediction of carbon dioxide solubility in ionic liquids using MLP and radial basis function (RBF) neural networks. *J. Taiwan Inst. Chem. Eng.* **60**, 151–164 (2016).
- Hamzehie, M. et al. Application of artificial neural networks for estimation of solubility of acid gases (H₂S and CO₂) in 32 commonly ionic liquid and amine solutions. *J. Nat. Gas Sci. Eng.* **24**, 106–114 (2015).
- Fierro, E. N. et al. Application of a single multilayer perceptron model to predict the solubility of CO₂ in different ionic liquids for gas removal processes. *Processes* **10**(9), 1686 (2022).
- Nassef, A. M. Improving CO₂ absorption using artificial intelligence and modern optimization for a sustainable environment. *Sustainability* **15**(12), 9512 (2023).
- Wang, K. et al. Machine learning-based ionic liquids design and process simulation for CO₂ separation from flue gas. *Green Energy Env.* **6**(3), 432–443 (2021).
- Ali, M. et al. Prediction of CO₂ solubility in Ionic liquids for CO₂ capture using deep learning models. *Sci. Rep.* **14**(1), 14730 (2024).
- Rahimi, A., Bahmanzadegan, F. & Ghaemi, A. Analysis of CO₂ solubility in ionic liquids as promising absorbents using response surface methodology and machine learning. *J. CO₂ Utiliz.* **93**, 103043 (2025).
- Anthony, J. L., Maginn, E. J. & Brennecke, J. F. Solubilities and thermodynamic properties of gases in the ionic liquid 1-n-butyl-3-methylimidazolium hexafluorophosphate. *J. Phys. Chem. B* **106**(29), 7315–7320 (2002).
- Aki, S. N. et al. High-pressure phase behavior of carbon dioxide with imidazolium-based ionic liquids. *J. Phys. Chem. B* **108**(52), 20355–20365 (2004).
- Pérez-Salado Kamps, Á. et al. Solubility of CO₂ in the ionic liquid [bmim][PF₆]. *J. Chem. Eng. Data* **48**(3), 746–749 (2003).
- Yokozeki, A. et al. Physical and chemical absorptions of carbon dioxide in room-temperature ionic liquids. *J. Phys. Chem. B* **112**(51), 16654–16663 (2008).
- Freitas, A. et al. Modeling vapor liquid equilibrium of ionic liquids+ gas binary systems at high pressure with cubic equations of state. *Braz. J. Chem. Eng.* **30**, 63–73 (2013).
- Gong, Y. et al. A high-pressure quartz spring method for measuring solubility and diffusivity of CO₂ in ionic liquids. *Ind. Eng. Chem. Res.* **52**(10), 3926–3932 (2013).
- Shiflett, M. B. & Yokozeki, A. Solubility and diffusivity of hydrofluorocarbons in room-temperature ionic liquids. *AIChE J.* **52**(3), 1205–1219 (2006).
- Shiflett, M. B. & Yokozeki, A. Solubilities and diffusivities of carbon dioxide in ionic liquids:[bmim][PF₆] and [bmim][BF₄]. *Ind. Eng. Chem. Res.* **44**(12), 4453–4464 (2005).
- Afzal, W., Liu, X. & Prausnitz, J. M. Solubilities of some gases in four imidazolium-based ionic liquids. *J. Chem. Thermodyn.* **63**, 88–94 (2013).
- Kodama, D. et al. Density, viscosity, and CO₂ solubility in the ionic liquid mixtures of [bmim][PF₆] and [bmim][TFSA] at 313.15 K. *J. Chem. Eng. Data* **63**(4), 1036–1043 (2017).
- Mazzer, H. R. et al. Phase behavior at high pressure of the ternary system: CO₂, ionic liquid and disperse dye. *J. Thermodyn.* **2012**(1), 921693 (2012).
- Gonzalez-Miquel, M. et al. Anion effects on kinetics and thermodynamics of CO₂ absorption in ionic liquids. *J. Phys. Chem. B* **117**(12), 3398–3406 (2013).
- Shiflett, M. B. & Yokozeki, A. Separation of CO₂ and H₂S using room-temperature ionic liquid [bmim][PF₆]. *Fluid Phase Equilib.* **294**(1–2), 105–113 (2010).

43. Altowayti, W. A. H. et al. The removal of arsenic species from aqueous solution by indigenous microbes: batch bioadsorption and artificial neural network model. *Environ. Technol. Innov.* **19**, 100830 (2020).
44. Pashaei, H., Mashhadimoslem, H. & Ghaemi, A. Modeling and optimization of CO₂ mass transfer flux into Pz-KOH-CO₂ system using RSM and ANN. *Sci. Rep.* **13**(1), 4011 (2023).
45. Masoumi, H. et al. Modeling of carbon dioxide absorption into aqueous alkanolamines using machine learning and response surface methodology. *Sci. Rep.* **14**(1), 23967 (2024).
46. Naeem, S., Shahhosseini, S. & Ghaemi, A. Simulation of CO₂ capture using sodium hydroxide solid sorbent in a fluidized bed reactor by a multi-layer perceptron neural network. *J. Nat. Gas Sci. Eng.* **31**, 305–312 (2016).
47. Vaferi, B., Eslamloueyan, R. & Ayatollahi, S. Automatic recognition of oil reservoir models from well testing data by using multi-layer perceptron networks. *J. Petrol. Sci. Eng.* **77**(3–4), 254–262 (2011).
48. Yang, L. & Zhang, C.-L. Modified neural network correlation of refrigerant mass flow rates through adiabatic capillary and short tubes: Extension to CO₂ transcritical flow. *Int. J. Refrig.* **32**(6), 1293–1301 (2009).
49. Majdi, A. & Beiki, M. Evolving neural network using a genetic algorithm for predicting the deformation modulus of rock masses. *Int. J. Rock Mech. Min. Sci.* **47**(2), 246–253 (2010).
50. Jin, R. et al. Energy saving strategy of the variable-speed variable-displacement pump unit based on neural network. *Procedia CIRP* **80**, 84–88 (2019).
51. Liu, T.-I. & Jolley, B. Tool condition monitoring (TCM) using neural networks. *Int. J. Adv. Manuf. Technol.* **78**, 1999–2007 (2015).
52. Pashazadeh, H., Gheisari, Y. & Hamed, M. Statistical modeling and optimization of resistance spot welding process parameters using neural networks and multi-objective genetic algorithm. *J. Intell. Manuf.* **27**, 549–559 (2016).
53. Haris, S. M. & Mohammadi, H. Cantilever beam natural frequency prediction using artificial neural networks. In *Proceedings of SAI Intelligent Systems Conference (IntelliSys) 2016: Volume 2* (Springer, 2018).
54. Oreta, A. W. C. Bond strength prediction model of corroded reinforcement in concrete using neural network. *GEOMATE J.* **16**(54), 55–61 (2019).
55. Carroll, J. J., Slupsky, J. D. & Mather, A. E. The solubility of carbon dioxide in water at low pressure. *J. Phys. Chem. Ref. Data* **20**(6), 1201–1209 (1991).

Author contributions

Hadiseh Masoumi: Data Curation, Writing—original draft, Methodology, Validation, Investigation, Resources. Bahador Daryayehsalameh: Writing—review & editing, Validation, Formal analysis, Resources. Ahad Ghaemi: Conceptualization, Methodology, Writing—review & editing, Supervision.

Funding

This research received no specific grant from any funding agency in the public, commercial, or not-for-profit sectors.

Declarations

Competing interests

The authors declare no competing interests.

Additional information

Supplementary Information The online version contains supplementary material available at <https://doi.org/10.1038/s41598-025-31299-1>.

Correspondence and requests for materials should be addressed to H.M. or A.G.

Reprints and permissions information is available at www.nature.com/reprints.

Publisher's note Springer Nature remains neutral with regard to jurisdictional claims in published maps and institutional affiliations.

Open Access This article is licensed under a Creative Commons Attribution-NonCommercial-NoDerivatives 4.0 International License, which permits any non-commercial use, sharing, distribution and reproduction in any medium or format, as long as you give appropriate credit to the original author(s) and the source, provide a link to the Creative Commons licence, and indicate if you modified the licensed material. You do not have permission under this licence to share adapted material derived from this article or parts of it. The images or other third party material in this article are included in the article's Creative Commons licence, unless indicated otherwise in a credit line to the material. If material is not included in the article's Creative Commons licence and your intended use is not permitted by statutory regulation or exceeds the permitted use, you will need to obtain permission directly from the copyright holder. To view a copy of this licence, visit <http://creativecommons.org/licenses/by-nc-nd/4.0/>.

© The Author(s) 2025